Materials Advances

Accepted Manuscript

This article can be cited before page numbers have been issued, to do this please use: M. Irshad, M. Asif, M. S. Butt, M. Rafique, M. Durrani and A. M. Fouda, *Mater. Adv.*, 2025, DOI: 10.1039/D4MA01199F.

ROYAL SOCIETY OF CHEMISTRY

rsc.li/materials-advances

View Article Online
DOI: 10.1039/D4MA01199F

Novel Bio-Chelating Agent-Assisted Eco-Friendly Synthesis of $Sr_{0.9}X_{0.1}CoO_{3-\delta}$ (X=Ba, Ce) Perovskite Electrodes for Super Capacitor Applications

Muneeb Irshad [1 *], Muhammad Asif [1], Muhammad Salim Butt [2], Muhammad Rafique [3], Misbah Durrani [1], Ahmed M. Fouda [4]

1. Department of Physics, University of Engineering and Technology, Lahore 54890, Pakistan.
2. Department of Electrical Engineering, University of Engineering and Technology, New Campus, Lahore 39021, Pakistan.
3. Department of Physics, University of Sahiwal, Sahiwal 57000, Pakistan.
4. Department of Chemistry, Faculty of Science, King Khalid University, Abha, Saudi Arabia

* Corresponding Author:
Muneeb Irshad (muneebirshad@gmail.com; muneeb_irshad@uet.edu.pk)

Highlights

- Developed an innovative eco-friendly synthesis approach utilizing the synergy of bio-chelating agent and biomolecules present in lemon, yielding $Sr_{0.9}X_{0.1}CoO_{3-\delta}$ (X=Ba, Ce) perovskite materials with reduced impurities and improved crystallinity relative to conventional green synthesis approach.

- The cubic perovskite structure was verified without secondary phases using XRD, while EDX and FTIR proved the accurate composition and functional group integrity of materials produced through a novel eco-friendly route for perovskite materials.

- Attained a significant specific capacitance for $Sr_{0.9}X_{0.1}CoO_{3-\delta}$ (X= Ce), synthesized through a semi-green methodology, thereby substantiating its viability as an effective electrode material for supercapacitor applications.

View Article Online
DOI: 10.1039/D4MA01199F

View Article Online
DOI: 10.1039/D4MA01199F

Abstract:

The current work pioneers the synthesis of a novel composition of $Sr_{0.9}X_{0.1}CoO_{3-\delta}$ (X = Ba, Ce) perovskite electrode materials for supercapacitors through an innovative semi-green route using lemon powder as the bio-chelating agent. The synergy between biomolecules and organic citric acid in lemon powder resulted in minimal impurities and enhanced the crystallinity of the desired perovskite electrodes. XRD analysis confirmed the cubic perovskite structure of all $Sr_{0.9}X_{0.1}CoO_{3-\delta}$ (X=Ba, Ce) perovskite electrodes synthesized via both semi-green and chemical approaches. Notably, samples synthesized through a semi-green approach exhibited better crystallinity with no secondary phase. Microstructural analysis revealed a dense and agglomerated morphology for all samples, while EDX analysis confirmed the elemental composition with no prominent impurities. FTIR analysis confirmed the presence of identical functional groups for samples synthesized with both routes. Electrochemical studies demonstrated the highest specific capacitance of 1176.36 Fg^{-1} and excellent electrochemical stability, with 88.2% capacity retention after 5000 galvanostatic charge-discharge cycles for $Sr_{0.9}X_{0.1}CoO_{3-\delta}$ (X=Ce) synthesized through a semi-green route. Meanwhile, $Sr_{0.9}X_{0.1}CoO_{3-\delta}$ (X=Ba) also depicted reasonable specific capacitance. These findings confirm that not only can the novel perovskite composition $Sr_{0.9}X_{0.1}CoO_{3-\delta}$ (X=Ba, Ce) be successfully utilized for supercapacitor applications, but the innovative semi-green can also be employed for the efficient synthesis of perovskite materials. ensuring minimal ecological impact and reduced impurities associated with conventional chemical and green synthesis routes, respectively.

Keywords: Semi-green, Perovskite, Supercapacitor, Microstructure

1. Introduction:

In the modern era, there is a dire need to explore energy devices that should be sustainable, environmentally friendly, and quickly responsive with high energy density and power density[1]. Supercapacitors (SC's) have emerged in recent years as promising energy storage technology due to their high cyclic stability, high power density, and fast charging/discharging rates [2–4] Many applications require high power instead of high energy, such as phone chargers, regenerative braking systems, and portable vacuum cleaners [5,6]. Therefore, supercapacitors can be used instead of conventional lithium-ion batteries [7]. Supercapacitors are intermediate between conventional

View Article Online
DOI: 10.1039/D4MA01199F

capacitors and rechargeable batteries but have a similar configuration with two electrodes, i.e., anode and cathode immersed in an electrolyte and a separator membrane [8].

There are two types of supercapacitors based on the charge storage mechanism: electrical double-layer capacitors (EDLCs) and pseudo capacitors [9,10]. In EDLC, charge is stored electro-statically at the interface between the electrolyte and surface of electrodes without any faradaic reaction (so-called non-faradaic). During the charging, the ions present in the electrolyte move towards their respective electrodes, and an inner Helmholtz layer is formed called a double layer, which enhances the specific capacitance [11–13]. In pseudo capacitors, the charge storage mechanism is accomplished by redox reaction (oxidation-reduction reaction), electrosorption, or ion intercalation mechanisms [14]. Thus, pseudo capacitors store charge both electrostatically as well as electrochemically, leading to higher specific capacitance than EDLCs. Carbon-based materials are used as electrode materials in EDLCs due to their facile processing, chemical stability, operational temperature range, use without binder agents, and well-established activation techniques [15]. EDLC stores the charge at their electrochemical surfaces; however, low energy density and specific capacitance, along with excessive cost, are the major drawbacks of EDLCs [13,16]. Pseudo-capacitive type materials, on the other hand, exhibit higher energy density but possess shorter life cycles. This limitation can be overcome by conductive, sustainable approaches to synthesize transition metal oxides [17]. Chi-Chang Hu et al., reported that RuO was the first transition metal oxide that showed pseudocapacitive behavior due to its various corrosive states that make the faradaic process possible. However, these transition metal oxides are too costly [18,19]. Perovskite oxides have gained significant attraction for different applications and now as potential electrode materials in supercapacitors due to their structural flexibility, low cost, high charge carrier mobility, compositional and stoichiometric flexibility, high tapping density, and appropriate oxygen vacancies [9,20]. The presence of oxygen vacancies in perovskite-based materials makes the intercalation process faster than transition metal oxides. Various perovskite oxides have been investigated as an active material for SCs due to a high number of oxygen vacancies and tapping density [21]. Recently, SrCoO has been explored as a potential electrode material for supercapacitors. It has been reported that $SrCoO_{3-\delta}$ perovskite with cubic structure exhibits higher conductivity than other structures, but it is hard to get structural stability at room temperatures [22]. Researchers have reported that with the help of different dopants at the A or B site, the $SrCoO_{3-\delta}$ can attain structural stability. It has been found that substitution of a mere 5% can introduce significant changes in the

View Article Online
DOI: 10.1039/D4MA01199F

conductivities, structure, and oxygen diffusion of perovskite structures. It is also reported that dopants such as Ce^{4+}, Y^{4+}, Zr^{4+}, Al^{3+}, and Sc^{3+} can increase oxygen permeability and conductivity by 1–2 orders of magnitude of perovskites due to high concentrations of oxygen vacancies [23–26]. The doping of SrCoO with Ba and Ce is expected to have a significant impact on the structural stability and conductivity of the $SrCoO_{3-\delta}$. It is reported that larger ionic radii of Ba ions than Sr can cause lattice distortions that lead toward the formation of higher oxygen vacancies to maintain charge neutrality [27]. Similarly, Ce doping can lead to the formation of oxygen vacancies. This is because Ce can exist in multiple oxidation states, primarily Ce^{3+} and Ce^{4+}. The transition between these states can lead to the formation or annihilation of oxygen vacancies to maintain charge neutrality [28]. Generally, the charge storage capacity of the perovskites is dependent upon the availability of the oxygen vacancies; therefore, doping of Ba and Ce in the $SrCoO_{3-\delta}$ will not only increase electrochemical performance as supercapacitor electrodes but at the same time will also improve its structural stability [29,30].

In addition to a novel composition of $Sr_{0.9}X_{0.1}CoO_{3-\delta}$ (X=Ba, Ce) as perovskite electrodes for supercapacitors, the current project also involves an innovative synthesis approach in which the synergetic role of organic citric acid (lemon) and biomolecules as reducing and capping agents are used to synthesize $Sr_{0.9}X_{0.1}CoO_{3-\delta}$ (X=Ba, Ce) for the first time. Although chemical approaches are commonly used to synthesize perovskites, they involve the use of hazardous solvents and reagents, causing substantial ecological and health concerns [31]. In contrast, the green approach can mitigate these concerns, but the end product through the green approach lacks phase purity and desired crystallinity, reduced reproducibility, and lower yield [32]. Therefore, balancing the efficiency and environmental impact of both synthesis routes remains a critical challenge in the advancement of perovskite technology. The proposed novel approach can attain this balance by simultaneously utilizing the reducing and capping role of both biomolecules and organic citric acid present in the lemon to synthesize $Sr_{0.9}X_{0.1}CoO_{3-\delta}$ (X=Ba, Ce) perovskite electrode.

Herein, $Sr_{0.9}X_{0.1}CoO_{3-\delta}$ (X=Ba, Ce) perovskite composition is synthesized for the first time as electrodes for pseudocapacitive applications. In addition, an innovative semi-green approach is also employed to synthesize this novel composition along with a conventional chemical approach. This novel semi-green approach utilizes the synergy of biomolecules and organic citric acid present in the lemon as reducing and capping agents, therefore providing more control over the

View Article Online
DOI: 10.1039/D4MA01199F

synthesis process with minimized toxicity compared to the conventional approach and impurities compared to the green approach. The synthesized electrodes were investigated through various characterizations.

2. Experimentation

Semi-green and chemical combustion methods were employed to synthesize $Sr_{0.9}X_{0.1}CoO_{3-\delta}$ (X=Ba, Ce) as the anode materials for supercapacitors. Starting precursors Sr $(NO_3)_2$, Co $(NO_3)_2.6H_2O$, Ba $(NO_3)_2.6H_2O$, and Ce $(NO_3)_2.6\ H_2O$ in exact stoichiometric ratio were dissolved in 200mL deionized water under constant stirring and heating to prepare a transparent solution. Lemon powder (LP) and citric acid (CA) were used as the chelating agent with 20-21 weight % of the total precursor solution. After being made in a ceramic beaker, the clear precursor solution was put on a magnetic hot plate. The solution was continuously stirred and heated at 80^0C on a hot plate. The viscosity of that homogeneous solution was increased by the boiling of water and changed into gel at 110^0C. Further heating evaporated all the water from the pores of the gel and was self-ignited to produce a fine powder of perovskite materials. The obtained powder is then calcinated at 200^0C for 1 hour and sintered at 1150^0C for 5 hours to obtain further fine powder. Pellets of sintered powder were formed by using a hydraulic press under pressure of 300 MPa and are then characterized by different techniques such as XRD, FESEM, EDX, FTIR, CV and GCD.

View Article Online
DOI: 10.1039/D4MA01199F

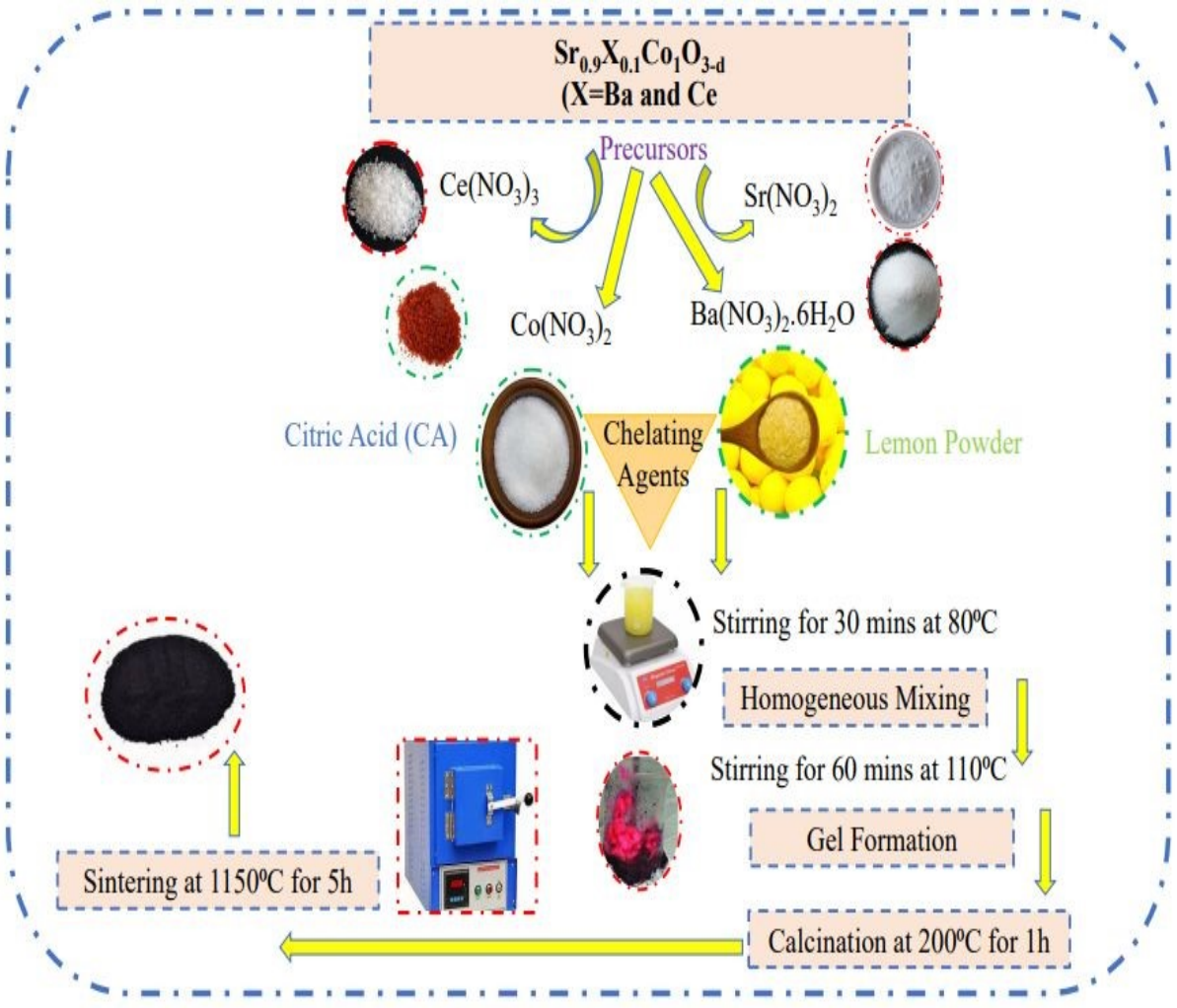

Figure 1. Schematic representation of $Sr_{0.9}X_{0.1}CoO_{3-\delta}$ (X=Ba, Ce) perovskite anode materials synthesized through semi-green (LP) and chemical (CA) approaches

All the synthesized were characterized samples using X-ray diffraction (XRD), scanning electron microscopy (SEM), energy dispersive x-ray spectroscopy (EDX) and Fourier-transform infrared spectroscopy (FTIR) to study the structural properties, morphology, elemental composition, and functional groups. The electrochemical performance of the synthesized electrodes was observed using a 1M KOH electrolyte solution by using voltammetry CV and GCD.

3. Results and Discussions

Figure 1(a). represents XRD spectra of $Sr_{0.9}X_{0.1}CoO_{3-\delta}$ (X=Ba, Ce) synthesized through semi-green (LP) and chemical (CA) approaches. The diffraction planes (100), (101), (110), (111), (200), (211), (220) and (221) confirming their cubic structure (JCPDS=00-038-1148) with the space

View Article Online
DOI: 10.1039/D4MA01199F

group of Pm3m were observed in all samples $Sr_{0.9}X_{0.1}CoO_{3-\delta}$ (X=Ba, Ce) synthesized either through semi-green (LP) or chemical (CA) approach.

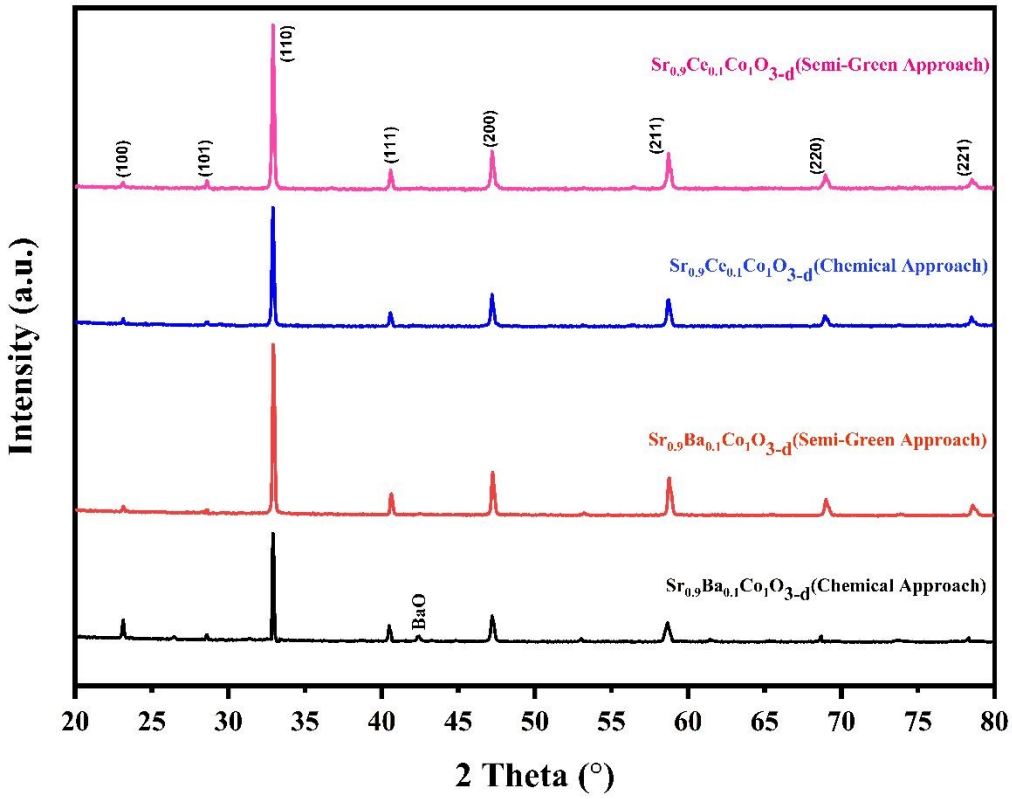

Figure 2. XRD Spectra of $Sr_{0.9}X_{0.1}CoO_{3-\delta}$ (X=Ba, Ce) synthesized through semi-green and chemical approaches representing cubic perovskite structure for all the samples with no extra phases, however, a small BaO phase appeared for $Sr_{0.9}Ba_{0.1}O_{3-\delta}$ synthesized through chemical approach.

It is clear that $Sr_{0.9}X_{0.1}CoO_{3-\delta}$ synthesized with semi-green (LP) synthesis exhibited no secondary phases, however, it is interesting to observe that $Sr_{0.9}X_{0.1}CoO_{3-\delta}$ (X=Ba) synthesized with a chemical approach exhibited a secondary phase of BaO, which was unexpected for the chemical approach. The presence of a secondary phase can be attributed to the low sintering temperature as reported by researchers where the BaO phase appeared for samples sintered at temperatures lower than 1400°C [33–38]. The absence of BaO in $Sr_{0.9}X_{0.1}CoO_{3-\delta}$ (X=Ba) synthesized with a semi-green (LP) approach can be credited to the presence of metallic impurities, which may have acted as a sintering aid.

View Article Online
DOI: 10.1039/D4MA01199F

Table 1 represents the variation in structural parameters such as crystalline size, dislocation density, microstrain, and lattice constant for $Sr_{0.9}X_{0.1}Co\ O_{3-\delta}$ synthesized through semi-green (LP) and chemical (CA) approaches.

Table 1. Structural parameters of $Sr_{0.9}X_{0.1}CoO_{3-\delta}$ perovskite anode representing larger crystallite size for semi-greenly (LP) synthesized anodes as compared to chemically (CA) synthesized anodes.

Sample	Crystalline Size (nm)	Lattice constant (nm)	Dislocation Density (m^{-2})	Microstrain (nm)
$Sr_{0.9}Ce_{0.1}CoO$ (Semi-green Method)	49	0.072731	0.401214	0.002452
$Sr_{0.9}Ce_{0.1}CoO$ (Chemical Method)	47	0.072745	0.446863	0.002586
$Sr_{0.9}Ba_{0.1}CoO$ (Semi-green Method)	56	0.072764	0.317514	0.00218
$Sr_{0.9}Ba_{0.1}CoO$ (Chemical Method)	52	0.072804	0.367166	0.002343

Figure 3. (a, b) represents the crystallite size and lattice constant of $Sr_{0.9}X_{0.1}Co\ O_{3-\delta}$ (X=Ba, Ce) perovskite anode synthesized through semi-green (LP) and chemical (CA) routes. It is clear from figure 3. (a) that crystallite size of $Sr_{0.9}X_{0.1}Co\ O_{3-\delta}$ (X=Ba, Ce) synthesized by semi-green (LP) approach is larger than the chemical (CA) and can be ascribed to the fact that LP contains metallic impurities like Mg and Ca which may acted as sintering aid due to which crystals starts diffusing hence crystalline size increases [39–41].

It can be further inferred from the table 1 and figure 3 (a) that among semi-greenly (LP) and chemically (CA) synthesized $Sr_{0.9}X_{0.1}Co\ O_{3-\delta}$ and $Sr_{0.9}Ba_{0.1}CoO_{3-\delta,}$ the $Sr_{0.9}Ba_{0.1}CoO_{3-\delta}$ exhibited larger crystallite size compared to $Sr_{0.9}Ce_{0.1}CoO_{3-\delta}$ which implies that Ba has larger ionic radii and its incorporation in the lattice occupy the interstitial sites that leads to lattice expansion and larger grain boundaries [42]. Another reason for the small crystallite of $Sr_{0.9}Ce_{0.1}CoO_{3-\delta}$ compared to $Sr_{0.9}Ba_{0.1}CoO_{3-\delta}$ is the small ionic radii of Ce, resulting in the effective incorporation of Ce into the lattice which may enhance the grain boundary formation and inhibit the grain growth, leading to finer crystallites [43].

Similarly, figure 3. (b) represents the variation of the lattice constant of $Sr_{0.9}X_{0.1}CoO_{3-\delta}$ (X=Ba, Ce) synthesized through semi-green (LP) and chemical (CA) approaches; showing a smaller lattice

View Article Online
DOI: 10.1039/D4MA01199F

constant for semi-green synthesis which may be ascribed to the fact that sustainable approach has improved the crystallinity leading to smaller defect densities in the lattice formation [44]. It can be further inferred from Table 1 and figure 3(b) that the $Sr_{0.9}Ce_{0.1}CoO_{3-\delta}$ has a smaller lattice constant compared to $Sr_{0.9}Ba_{0.1}CoO_{3-\delta}$ which is ascribed to a small difference in the ionic radii of Ce than the Ba [45].

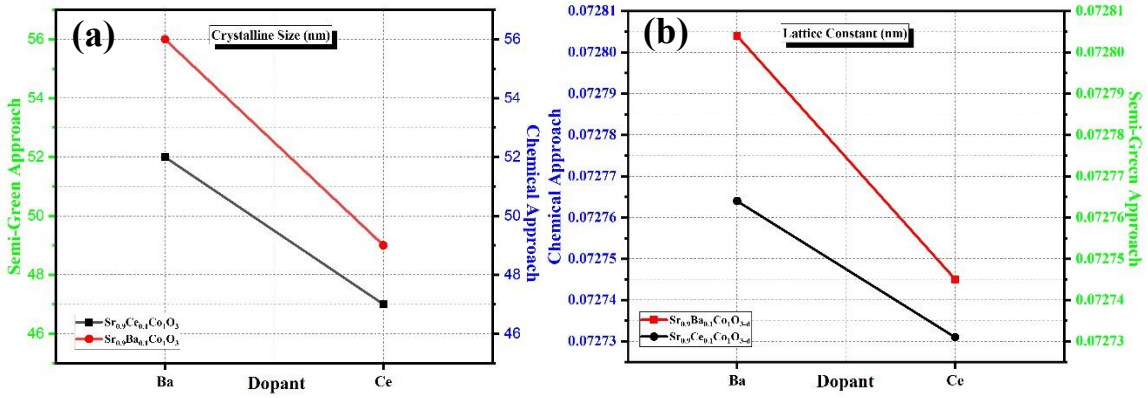

Figure 3. Variation of (a) crystalline size and (b) lattice constant for (110) plane of $Sr_{0.9}X_{0.1}CoO_{3-\delta}$ (X=Ba, Ce) synthesized through semi-green (LP) and chemical (CA) approaches.

Figure 4. (a, b) represents the variation of dislocation density and microstrain of $Sr_{0.9}X_{0.1}CoO_{3-d}$ (X=Ba, Ce) synthesized through two approaches. It is clear from figure 4. (a) that the dislocation density is higher for the semi-green (LP) method due to metallic impurities influencing the lattice symmetry and leading to larger dislocations [46]. It can be observed from the figure 4. (b) that samples synthesized by semi-green (LP) routes have larger micro strain compared to chemical (CA) due to metallic impurities like Mg and Ca; the semi-green method causes higher lattice distortions. Similarly, $Sr_{0.9}Ce_{0.1}CoO_{3-\delta}$ shows higher microstrain than $Sr_{0.9}Ba_{0.1}CoO_{3-\delta}$ which may be due to the higher valency of Ce^{3+} than Ba^{2+}, thus producing more oxygen vacancies resulting in higher lattice distortion in the unit cell [42,47] as shown in figure 4(b).

View Article Online
DOI: 10.1039/D4MA01199F

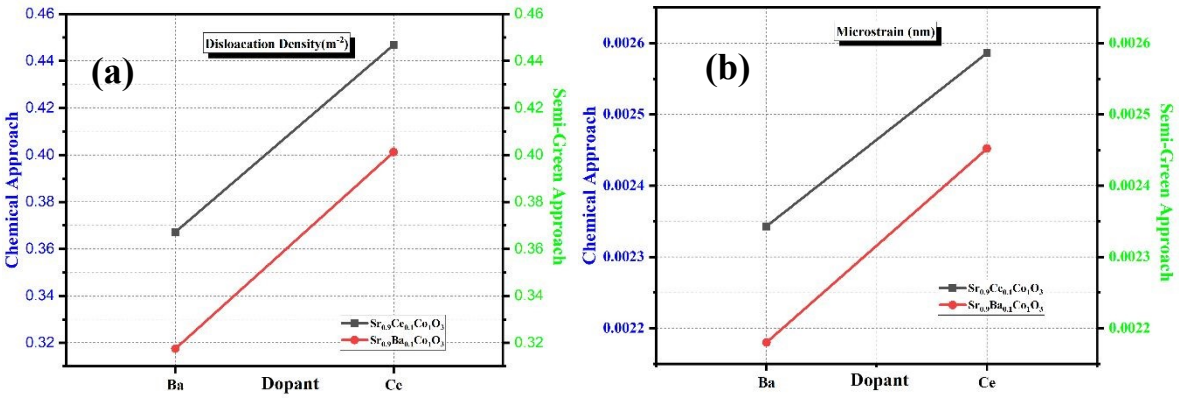

Figure 4. Variation of (a) dislocation density and (b) micro strain for (110) plane of $Sr_{0.9}X_{0.1}CoO_{3-\delta}$ (X=Ba, Ce) synthesized through semi-green (LP) and chemical (CA) approaches.

4. Scanning Electron Microscope (SEM)

Figure 5 (a-d) represents the micrographs of $Sr_{0.9}X_{0.1}CoO_{3-\delta}$ synthesized through semi-green (LP) and chemical (CA) routes, while figure 5 (e-h) represents their corresponding histogram. It is clear from the micrograph (Fig. 5a) of $Sr_{0.9}Ba_{0.1}CoO_{3-\delta}$ anode synthesized through semi-green (LP) approach that it exhibits a regular and porous structure with a more defined shape and less agglomeration compared to $Sr_{0.9}Ba_{0.1}CoO_{3-\delta}$ anode (Fig. 5b) synthesized with chemical (CA) approach which can be credited to the presence of biomolecules and organic citric acid present in the lemon powder. It is reported that biomolecules present in organic compounds act as the reducing and capping agents during the semi-green synthesis; therefore, the combined effect of organic citric acid and biomolecules present in the lemon powder will provide more control over the growth and agglomeration of the nanoparticles [48–50]. The microstructure of $Sr_{0.9}Ba_{0.1}CoO_{3-\delta}$ anode synthesized through the chemical method shows irregular particle shapes with multiple crevices and protrusions, indicating the heterogeneous nature of the particles. Figure 5 (e-f) shows the range of $Sr_{0.9}Ba_{0.1}CoO_{3-\delta}$ anode's particle sizes synthesized by two approaches. It is evident from the statistical histogram (Fig. 5e) that the particle size of $Sr_{0.9}Ba_{0.1}CoO_{3-\delta}$ synthesized through semi-green (LP) route ranges from 10–55 nm with maximum particles existing in the range 20–25 nm while $Sr_{0.9}Ba_{0.1}CoO_{3-\delta}$ anode synthesized through chemical (CA) route lies in the long-range from 10 – 110 nm particle with maximum particles existing in the range of 80 – 90nm. This variation in the particle sizes of synthesized $Sr_{0.9}Ba_{0.1}CoO_{3-\delta}$ through two routes clearly shows that

View Article Online
DOI: 10.1039/D4MA01199F

the collegial role of natural citric acid and biomolecules in the semi-green (LP) route effectively reduced and capped the $Sr_{0.9}Ba_{0.1}CoO_{3-\delta}$ compared to the chemical synthesis route, where only synthetic citric acid acted as a reducing and capping agent [51,52].

The microstructures of $Sr_{0.9}Ce_{0.1}CoO_{3-\delta}$ synthesized through both approaches are shown in Figure 5(c-d), while corresponding histograms for particle sizes are shown in Figure 5(g-h). The $Sr_{0.9}Ce_{0.1}CoO_{3-\delta}$ anode exhibited a similar pattern to that of $Sr_{0.9}Ba_{0.1}CoO_{3-\delta}$ that is $Sr_{0.9}Ce_{0.1}CoO_{3-\delta}$ anode particles synthesized through the semi-green (LP) route exhibited small and round particles with less agglomeration while chemically synthesized $Sr_{0.9}Ce_{0.1}CoO_{3-\delta}$ anode have larger and more agglomerated particles. The particle size of semi-greenly synthesized $Sr_{0.9}Ce_{0.1}CoO_{3-\delta}$ lies in 4 – 24 nm, while maximum particles exist in the range 8 – 12 nm, whereas the size of chemically synthesized particles ranges 10 - 120nm with maximum particles having a size of 40-50 nm.

It can be further inferred from the figures 5 (a-d) that among semi-greenly (LP) and chemically (CA) synthesized $Sr_{0.9}Ce_{0.1}CoO_{3-\delta}$ and $Sr_{0.9}Ba_{0.1}CoO_{3-\delta}$, the $Sr_{0.9}Ba_{0.1}CoO_{3-\delta}$ exhibited larger crystallite size compared to $Sr_{0.9}Ce_{0.1}CoO_{3-\delta}$ which implies that Ce ions in $Sr_{0.9}Ce_{0.1}CoO_{3-\delta}$ can act as nucleation sites, facilitating the production of nuclei during the synthesis process. Ce can accelerate crystal growth by occupying these favorable sites, providing stable anchoring points for precursor molecules to attach and arrange themselves, thus facilitating nucleation, resulting in the formation of smaller particles with a more uniform size distribution.

View Article Online
DOI: 10.1039/D4MA01199F

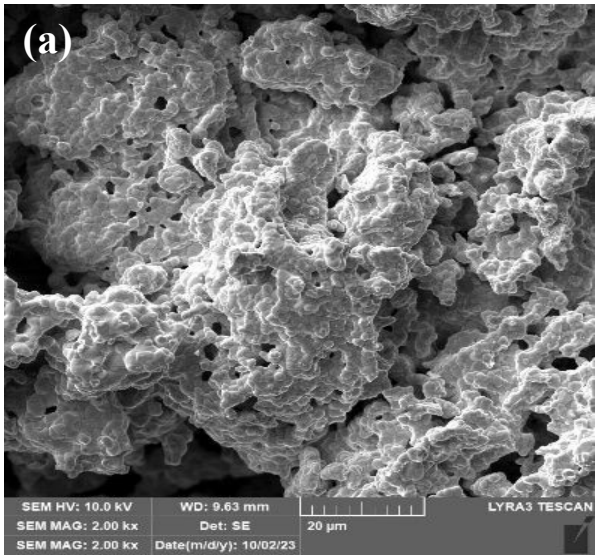

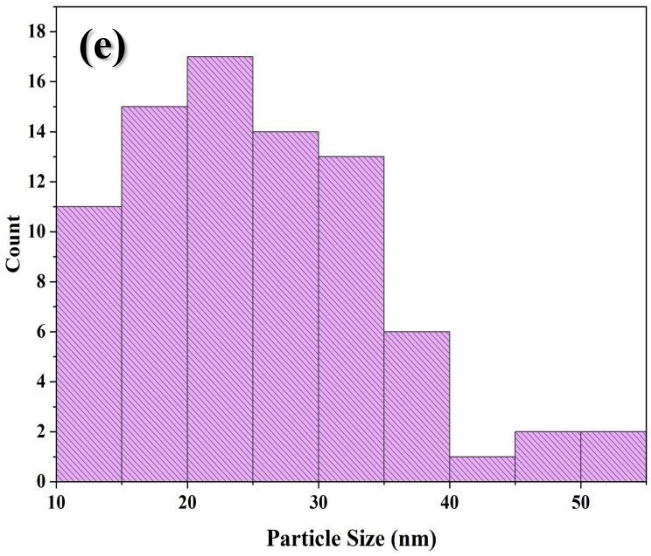

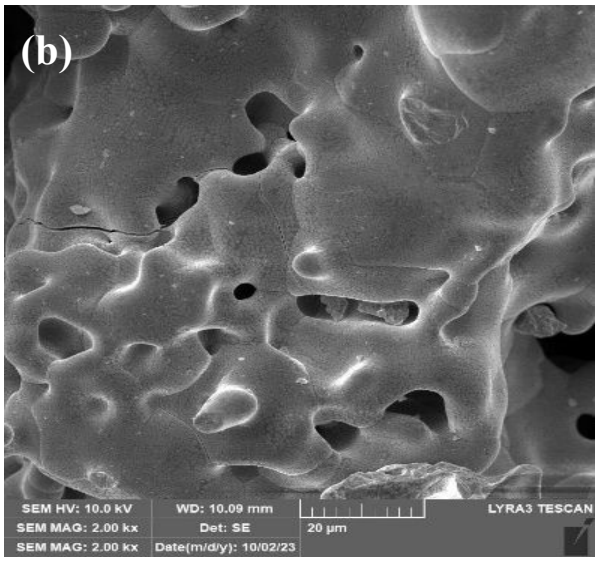

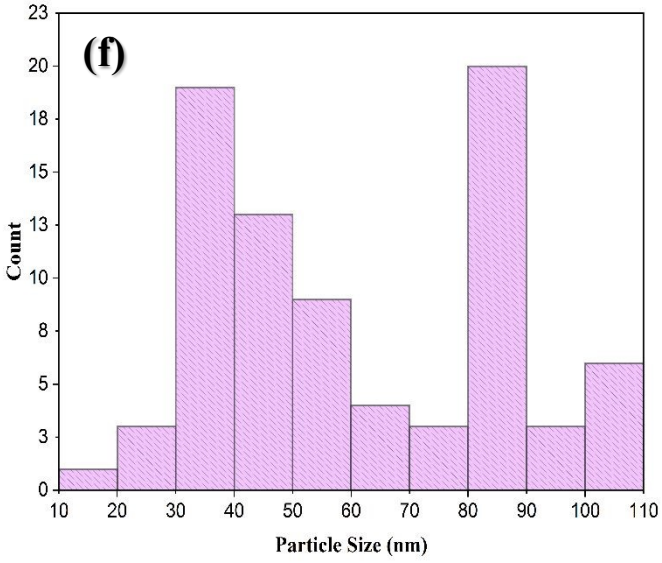

View Article Online
DOI: 10.1039/D4MA01199F

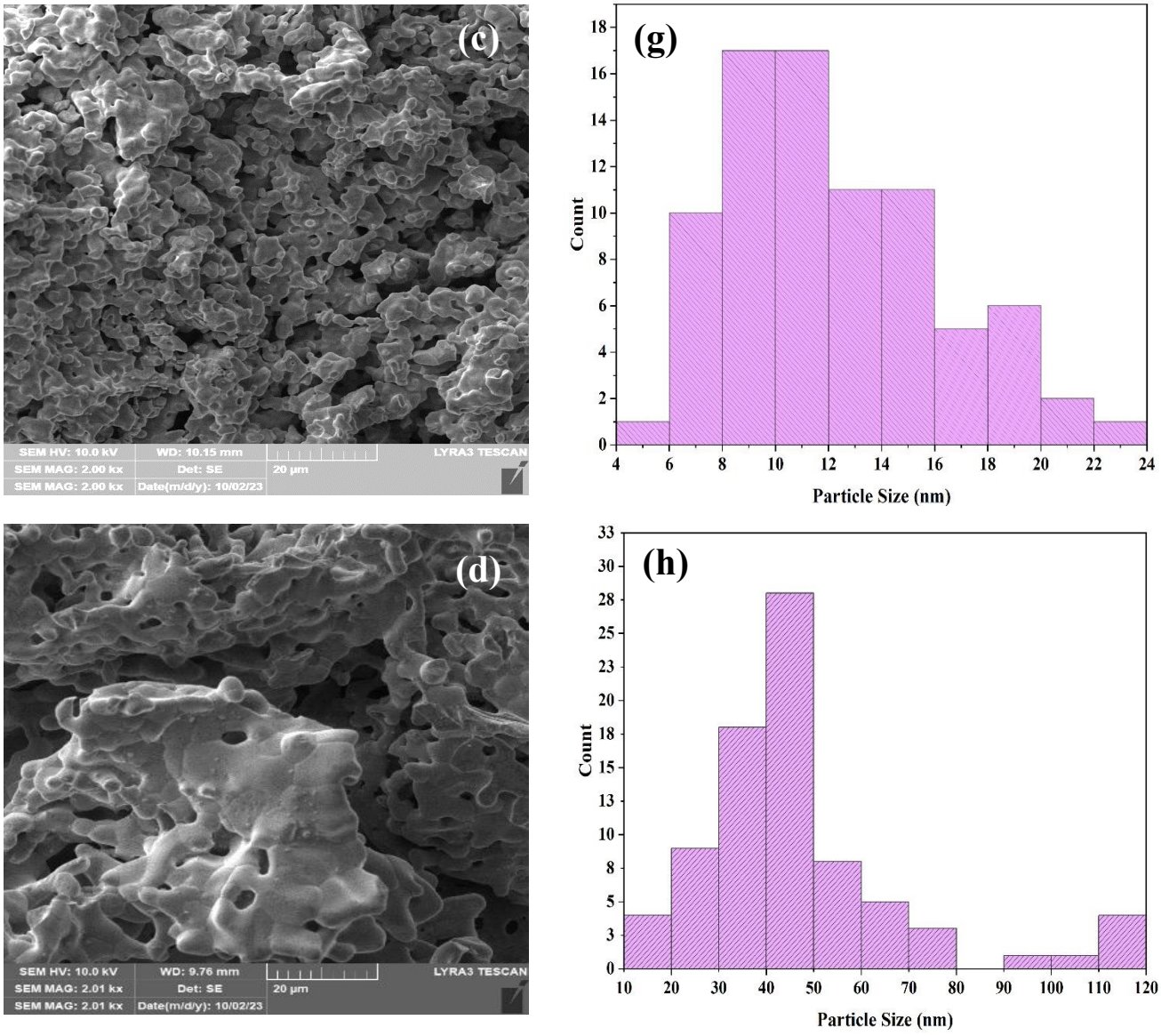

(Fig. 5a) of $Sr_{0.9}Ba_{0.1}CoO_{3-\delta}$ anode synthesized through semi-green (LP) approach that it exhibits a regular and porous structure, and (Fig. 5b) of $Sr_{0.9}Ba_{0.1}CoO_{3-\delta}$ anode synthesized through chemical (CA) approach showing agglomeration. (Fig. 5c) of $Sr_{0.9}Ce_{0.1}CoO_{3-\delta}$ anode synthesized through semi-green (LP) approach, and (Fig. 5d) of $Sr_{0.9}Ce_{0.1}CoO_{3-\delta}$ anode synthesized through chemical (CA) approach showing agglomeration.

View Article Online
DOI: 10.1039/D4MA01199F

5. EDX Analysis

Figure 6 (a-d) represents the EDX spectra of $Sr_{0.9}X_{0.1}CoO_{3-\delta}$ anode materials synthesized through semi-green (LP) and chemical (CA) routes. The surface areas were carefully selected for the EDX analysis to avoid surface contaminants. The qualitative spectra shown in Fig. 6 (a-d) confirmed the presence of strontium, cobalt, and oxygen in all samples, while Ba and Ce were confirmed in $Sr_{0.9}Ba_{0.1}CoO_{3-\delta}$ and $Sr_{0.9}Ce_{0.1}CoO_{3-\delta}$ synthesized by both routes, respectively. The quantitative spectra shown in the inset provide the percentage of the elemental composition for $Sr_{0.9}X_{0.1}CoO_{3-\delta}$ anode materials. It can also be observed from the spectra that no impurity-related peaks appeared, depicting the high purity of the $Sr_{0.9}X_{0.1}CoO_{3-\delta}$. The absence of impurity-related peaks was unexpected for $Sr_{0.9}X_{0.1}CoO_{3-\delta}$ synthesized through the semi-green (LP) approach because lemon powder contains several minerals, but their absence from the spectra can be ascribed to their concentration being lower than the detection limit of EDX [53,54]. The compositional analysis confirms that the semi-green (LP) route can be employed for the successful synthesis of $Sr_{0.9}X_{0.1}CoO_{3-\delta}$ anode without significant impurities.

View Article Online
DOI: 10.1039/D4MA01199F

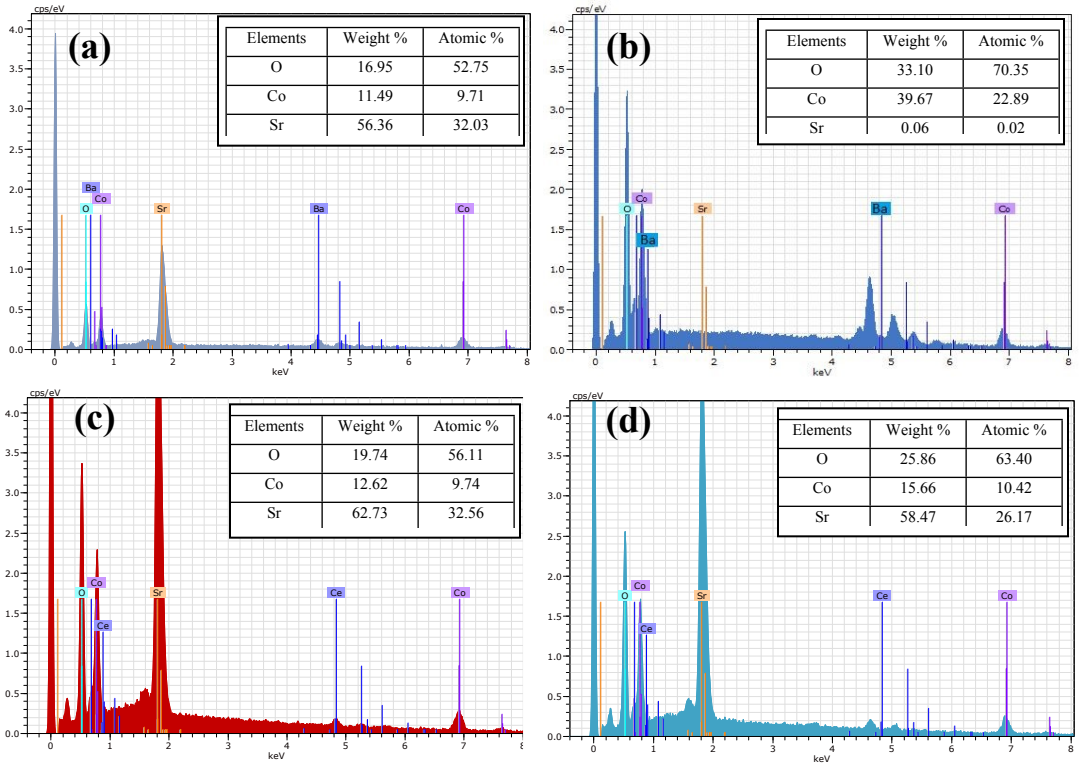

Figure 6. EDX spectrum of $Sr_{0.9}X_{0.1}CoO_{3-\delta}$ (a) doped with (X=Ba) using citric acid as chelating agent (b) doped with (X=Ba) lemon powder as chelating agent(c) doped with (X=Ce) using citric acid as chelating agent (d) doped with (X=Ce) lemon powder as chelating agent

6. Fourier Transform Infrared (FTIR) Analysis

Figure 7 depicts the FTIR spectra of $Sr_{0.9}X_{0.1}CoO_{3-\delta}$ (a) doped with Ba (b) doped with Ce, synthesized through citric acid and lemon powder as a chelating agent. The small peaks around 3735 cm^{-1}, 2980 cm^{-1}, 2361 cm^{-1},1461 cm^{-1}, and 994-911 cm^{-1} show the transmittance of O-H stretching, C-H stretching, O=C=O stretching, C-H bending and M-O stretching, respectively, in all the samples. Oxygen vacancies in perovskite oxides may cause hydroxyl groups (OH^-) to develop on the surface. These hydroxyl groups may have originated from the interaction of surface oxygen species with ambient moisture. Hydroxyl groups on the surface have produced O-H stretching vibrations in FTIR spectra [55]. C-H stretching and bending vibrations may arise due to the presence of organic residue within the synthesized material derived from the chelating agents used, i.e. citric acid and lemon powder. Peaks associated with O=C=O stretching vibrations imply the presence of carbonate species in the produced materials. The existence of carbonate species could be due to ambient CO_2 absorption or residual carbonate from precursor materials. There is

View Article Online
DOI: 10.1039/D4MA01199F

an indication of M-O stretching, which implies the formation of metal oxides, showing the perovskite nature of the samples, as researchers have reported [56–62].

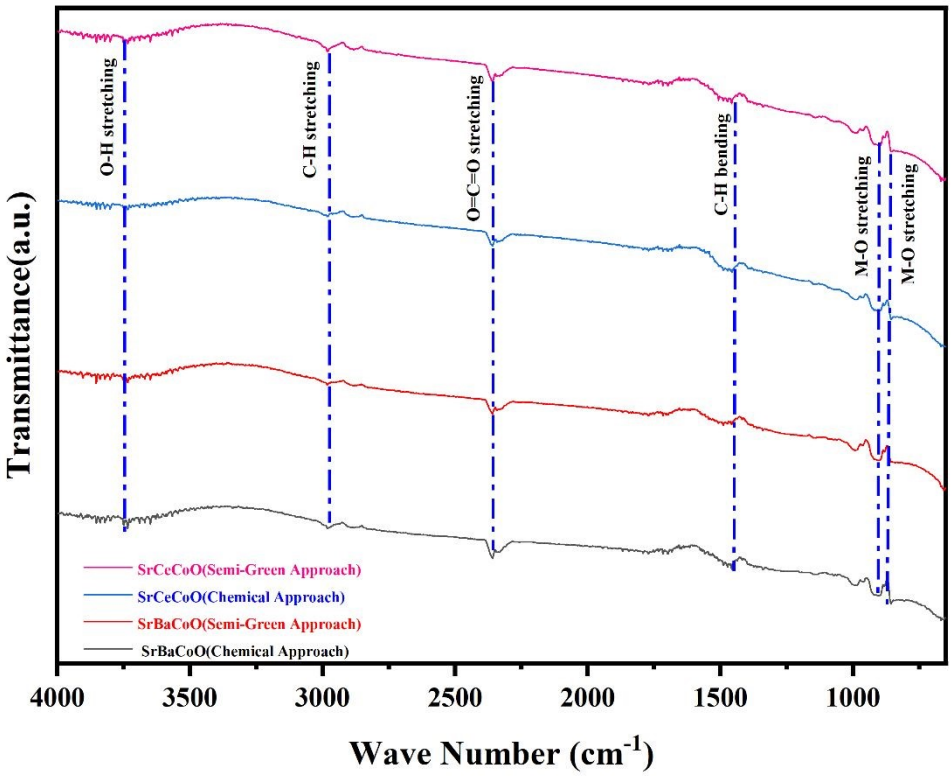

Figure 7. FTIR spectra of $Sr_{0.9}X_{0.1}CoO_{3-\delta}$ (a) doped with (X=Ba) (b) doped with (X=Ce) synthesized through semi-green (LP) and chemical (CA) approaches

7. Electrochemical Analysis:

a. Cyclic Voltammetry (CV):

The electrochemical performance of $Sr_{0.9}X_{0.1}CoO_{3-\delta}$ (X=Ba, Ce) perovskite electrodes synthesized through semi-green (LP) and chemical (CA) was evaluated through cyclic voltammetry and are shown in Fig. 8. Figure 8(a) displays the CV curves of $Sr_{0.9}X_{0.1}CoO_{3-\delta}$ (X=Ba, Ce) perovskite electrodes synthesized through semi-green (LP) and chemical (CA) in 1M KOH with a potential window range of 0.1-0.8V at a scan rate of 20 mV/s. It can be observed from CV curves that all materials exhibited pseudocapacitive behavior because of the faradaic redox reactions. Also, these curves depict rectangular and steep slopes, which suggest the higher power densities [63]. It is clear

View Article Online
DOI: 10.1039/D4MA01199F

from Fig. 8a that $Sr_{0.9}X_{0.1}CoO_{3-\delta}$ electrodes synthesized with a semi-green (LP) route exhibited better capacitance compared to the same electrodes synthesized through chemical (CA). The specific capacitance (Cs) of working electrodes was calculated using the equation [64]:

$$Cs = \frac{\int Idt}{2 \times M \times S \times \Delta V} \quad (1)$$

The specific capacitance of $Sr_{0.9}Ce_{0.1}CoO_{3-\delta}$ synthesized by semi-green (LP) and chemical (CA) approaches were 1176 Fg^{-1} and 871 Fg^{-1}, respectively, while $Sr_{0.9}Ba_{0.1}CoO_{3-\delta}$ synthesized through semi-green (LP) and chemical (CA) routes exhibited specific capacitance of 475 Fg^{-1} and 284 Fg^{-1} respectively and are depicted in Fig 8b. Figure 8. (c) shows the anodic and cathodic current peaks of $Sr_{0.9}X_{0.1}CoO_{3-d}$ (X=Ba, Ce) synthesized through both routes. It can be observed from Fig. 8 (a-c) that semi-greenly synthesized $Sr_{0.9}X_{0.1}CoO_{3-\delta}$ (X = Ba, Ce) electrodes exhibited better capacitance compared to corresponding chemically synthesized $Sr_{0.9}X_{0.1}CoO_{3-\delta}$ (X = Ba, Ce) which can be ascribed to presence of metallic impurities in the lemon powder which can facilitate the redox process due to availability of higher charge carriers. In addition, the large crystallite size of semi-greenly synthesized electrodes compared to chemically synthesized electrodes may also contribute to the better electrochemical performance [65]. Larger crystallite size leads to the reduction in the grain boundary resistance, which reduces the number of scattering sites. This permits the electrons to move freely through the material, enhancing the electrical conductivity, which facilitates the charge carriers to move faster, leading to rapid charging and discharging [66–68].

It is interesting to observed that among semi-greenly and chemically synthesized $Sr_{0.9}X_{0.1}CoO_{3-\delta}$ (X = Ba, Ce) electrodes, the $Sr_{0.9}Ce_{0.1}CoO_{3-\delta}$ electrode exhibited better performance compared to $Sr_{0.9}Ba_{0.1}CoO_{3-\delta}$ which can be ascribed to high valency states of Ce^{3+} than the Ba^{2+} therefore provides more charges leading to higher oxygen vacancies resulting in better electrochemical performance [69–71].

View Article Online
DOI: 10.1039/D4MA01199F

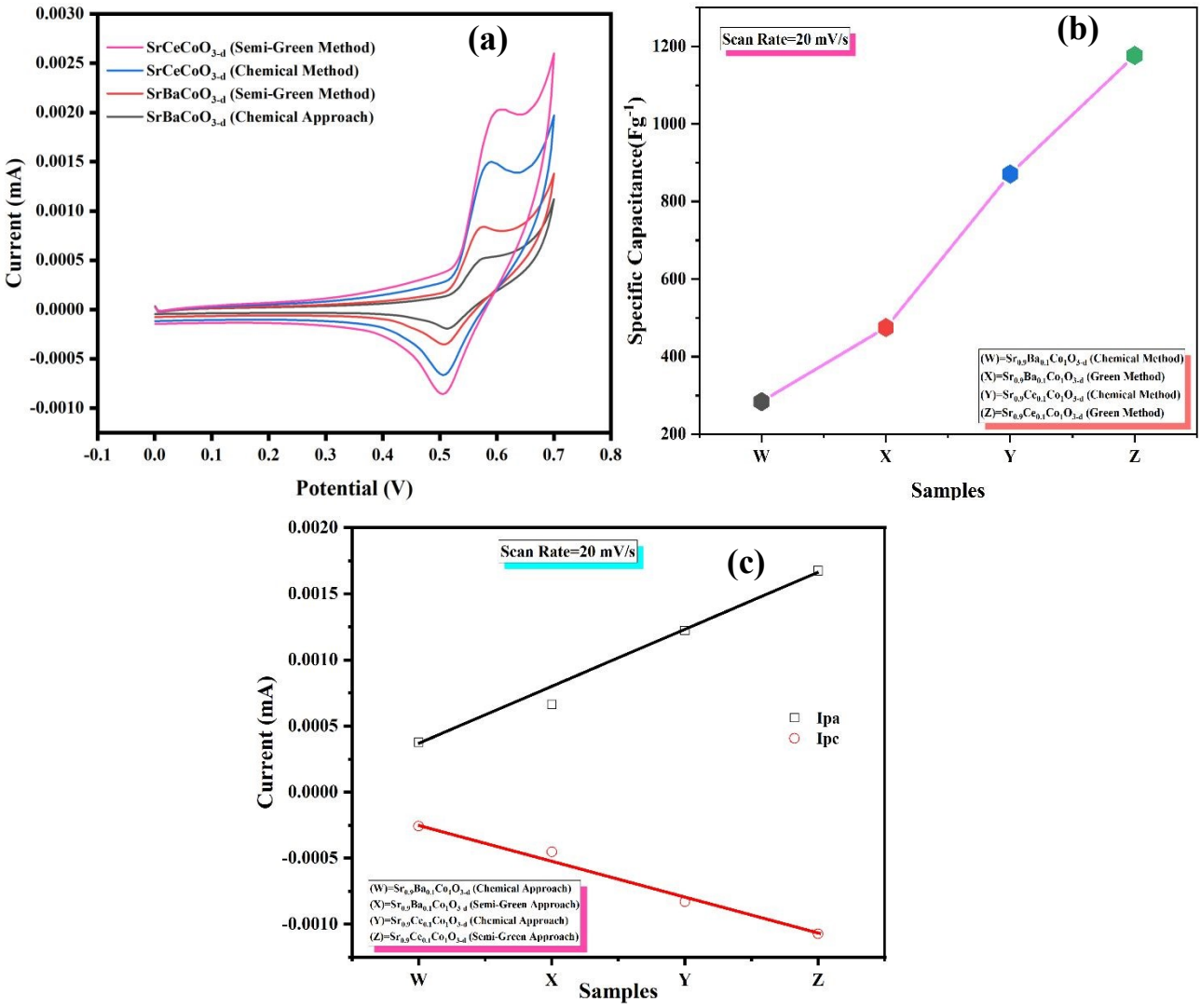

Figure 8. (a)Cyclic voltammetry curves of $Sr_{0.9}X_{0.1}CoO_{3-\delta}$ (X=Ba, Ce) with potential window range of -0.1-0.7 V at a scan rate of 20 mV/s (b) Specific Capacitance of $Sr_{0.9}X_{0.1}CoO_{3-\delta}$ (X=Ba, Ce) (c) Anodic and Cathodic peak currents from CV curves of $Sr_{0.9}X_{0.1}CoO_{3-\delta}$ (X=Ba, Ce)) synthesized through semi-green (LP) and chemical (CA) approaches

View Article Online
DOI: 10.1039/D4MA01199F

b. Galvanostatic Charge-Discharge (GCD)

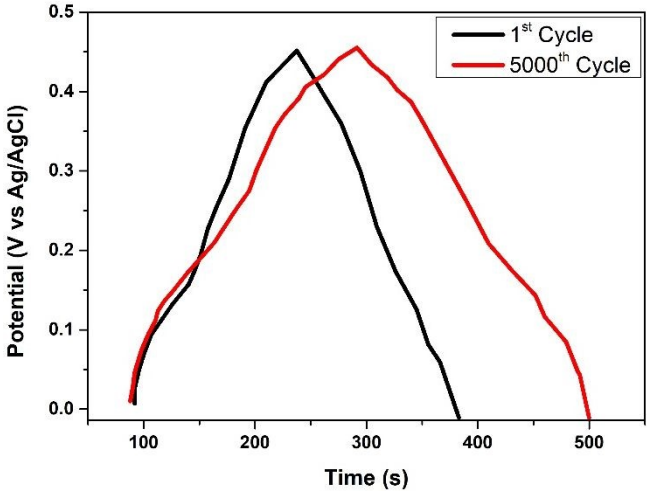

Figure 9. Galvanostatic charge-discharge (GCD) plot of $Sr_{0.9}X_{0.1}CoO_{3-\delta}$ (X= Ce) perovskite electrodes synthesized through semi-green (LP), comparing the electrochemical behavior between the 1st and 5000th cycles.

The GCD tests, as illustrated in Figure 9, were performed on $Sr_{0.9}X_{0.1}CoO_{3-\delta}$ (X=Ba, Ce) perovskite electrodes synthesized through semi-green (LP) and chemical (CA) approaches. These tests, conducted in a 1M KOH electrolyte within a 0–0.45 V potential window (vs. Ag/AgCl), compare the electrochemical behavior between the 1st and 5000th cycles. Figure 9 depicts the GCD curves for both synthesis methods, highlighting the material's impressive performance over extended cycling. Notably, the GCD tests revealed an exceptional 88.2% capacity retention after 5,000 cycles, as evidenced by the comparative curves in Figure 9. The semi-green synthesis of $Sr_{0.9}Ce_{0.1}CoO_{3-\delta}$ yielded a specific capacitance of 1176 F g^{-1} with 88.2% capacitance retention after 5,000 cycles, demonstrating performance comparable to, and in some instances surpassing, previously reported perovskite materials. For example, MnO_2@$SrCo_{0.875}Nb_{0.125}O_3$@CC exhibited a specific capacitance of 2066.0 mF cm^{-2} [72], while $SrFe_{0.85}Zr_{0.15}O_{3-\delta}$ achieved 163.92 F g^{-1} [73]. Similarly, Ti-substituted $SrCo_{0.9}Ti_{0.1}O_{3-\delta}$ delivered 625.0 F g^{-1}, attributed to its stable cubic structure and abundant oxygen vacancies [22]. Cr-substituted $SrCo_{0.95}Cr_{0.05}O_{3-\delta}$@CC, reported by Jiahao et al., maintained 95.8% capacitance after 10,000 cycles in an asymmetric configuration with PPy@CC [74]. Other perovskites, such as $SrCoO_{2.5}$ (475 F g^{-1}, 85% retention after 2,000 cycles) and $LaMnO_3$-based electrodes (720 F g^{-1}, 80% retention after 3,000 cycles), have also been

View Article Online
DOI: 10.1039/D4MA01199F

documented [29] [27]. Table 2 further provides comprehensive comparison among different supercapacitor electrodes.

Table 2: Comprehensive comparison among different electrodes

Electrode Material	**Cycling Stability (%)**	**Charge-Discharge Rate (A/g)**	**Operating Voltage Window (V)**	**Specific Capacitance (Fg^{-1})**	**Ref**
Ni3Se4/Co3Se4	83.4	1	1.5–1.8	1120.4	[75]
Reduced graphene oxide	97.14 (5000 cycles)	0.2	0.2–1.0	585.44	[76]
SbTe/SnSe	96.08 (5000 cycles)	1-3	0.1–0.7	1276	[77]
RGO/LaAlO3	55.47 (5000 cycles)	0.5	0–1.2	283	[78]
$La_{0.75}Sr_{0.25}Cr_{0.5}Mn_{0.5}O_3$ LSCM	92 (5000 cycles)	10	0.2–1.0	630	79

The enhanced stability obtained can be ascribed to the semi-green synthesis approach, which leverages lemon powder-derived biomolecules and citric acid to minimize agglomeration, enhance crystallinity (confirmed by XRD and SEM), reduce defects, and improve ionic conductivity. In contrast, chemically synthesized counterparts, such as $Sr_{0.9}Ba_{0.1}CoO_{3-\delta}$, suffer from accelerated capacity fading due to irregular morphologies and secondary phases (e.g., BaO). Furthermore, it also reflects the extraordinary structural integrity of our perovskite framework, even under repeated ion insertion and extraction. The selective substitution of strontium with barium and cerium enhances lattice stability and electrochemical reversibility, while the semi-green (LP) and chemical (CA) synthesis methods yield optimal particle shapes and crystallinity. These factors collectively minimize degradation mechanisms such as phase transitions or resistive layer formation, ensuring consistent performance over 5,000 cycles, as visually demonstrated in Figure

View Article Online
DOI: 10.1039/D4MA01199F

9. It is worth noting that 5,000 cycles is a widely accepted benchmark in energy storage research, providing a reliable indicator of material stability for preliminary evaluations. The superior performance of semi-green synthesized electrodes, as reflected in both the CV data and the GCD curves, can also be attributed to metallic impurities (e.g., Mg and Ca) from lemon powder, which boost redox processes, and larger crystallite sizes that reduce grain boundary resistance, enhancing electrical conductivity. In addition, the semi-green route followed for the synthesis of perovskite electrodes is more efficient compared to already existing green routes used to synthesize the perovskite electrodes for the supercapacitors. A comparative analysis of green routes is shown in Table 3.

Table 3: Performance Metrics of Green-Synthesized Perovskite-Based Supercapacitors

Electrode material	**Synthesis approach**	**Energy density (Wh kg^{-1})**	**Power density (W kg^{-1})**	**Specific capacitance (F/g)**	**Reference**
$LaMnO_3$	Green Synthesis (Lemon Juice)	52.5	1000	375	[80]
RGO/$LaAlO_3$	Green Synthesis (Green Tea)	57	569	721	[78]
Ag-Zirconia	Green Synthesis (Sauropus Androgynus)	31.94	500.86	256	[81]
$KMnCl_3/C_{60}$	Antisolvent (KCl and $MnCl_2$)	150.58	3.1	936	[82]
SnO_2/g-C_3N_4	Green Synthesis (Ananas comosus)	11.5	1705	302.7	[83]

The remarkable stability exhibited by $Sr_{0.9}X_{0.1}CoO_{3-\delta}$ (X= Ce) synthesized through semi-green route over 5,000 cycles, paired with high capacitance, can position these electrodes and the semi-

View Article Online
DOI: 10.1039/D4MA01199F

green routes as promising candidates for next-generation energy storage devices, where long-term operational reliability and sustainability is paramount.

Conclusions

In summary, the $Sr_{0.9}X_{0.1}CoO_{3-\delta}$ (X=Ba, Ce) are first-time synthesized as perovskite electrode materials for supercapacitors using an innovative semi-green approach leveraging lemon powder as a bio-chelating agent. This pioneering eco-friendly method achieved high-purity perovskite electrodes with minimal impurities, highlighting its potential for sustainable supercapacitor development. The synthesized electrodes were investigated and compared with chemically synthesized electrodes through XRD, FESEM, EDX, FTIR, and CV. The XRD validated the successful synthesis of the Ba and Ce doped $Sr_{0.9}X_{0.1}CoO_{3-\delta}$ perovskite structure through a semi-green approach with no secondary phase, as evidenced by the characteristic diffraction peaks. The FESEM micrographs revealed a homogenous microstructure with well-defined grains for semi-greenly synthesized $Sr_{0.9}X_{0.1}CoO_{3-\delta}$ (X=Ba, Ce), which was attributed to the collegial role of biomolecules and bio-chelating agents present in the lemon powder, while chemically synthesized perovskite anode exhibited irregular-shaped particles. The EDX mapping confirmed the presence of all elements in all samples synthesized by both approaches, while FTIR provided insights into the vibrational modes and confirmed the presence of the identical functional groups in all samples, further verifying the structural integrity of the materials synthesized by both approaches. Electrochemical performance evaluated by CV indicated that the semi-greenly synthesized $Sr_{0.9}X_{0.1}CoO_{3-\delta}$ (X=Ba, Ce) anodes exhibited promising redox behavior, with distinct oxidation and reduction peaks, compared to chemically synthesized anodes. It is also observed that Ce-doped $Sr_{0.9}X_{0.1}CoO_{3-\delta}$ exhibited better electrochemical performance than Ba-doped $Sr_{0.9}X_{0.1}CoO_{3-\delta}$, suggesting good potential for its application in energy storage and conversion devices. GCD of $Sr_{0.9}X_{0.1}CoO_{3-\delta}$ (X=Ce) perovskite electrodes exhibited remarkable electrochemical stability with 88.2% capacity retention after 5000 galvanostatic charge-discharge cycles, demonstrating that strategic A-site substitution effectively preserves the electrode's performance over extended cycling. In conclusion, it can be deduced that not only do $Sr_{0.9}X_{0.1}CoO_{3-\delta}$ (X=Ba, Ce) perovskite electrodes demonstrate significant potential as advanced materials for electrochemical storage applications, but the semi-green (LP) route can be effectively used as a synthesis approach for the synthesis of perovskite structure with minimal impurities and ecological impact.

View Article Online
DOI: 10.1039/D4MA01199F

Disclosure of Interest

The authors declare no competing or conflict of interest

Acknowledgment

The authors extend their appreciation to the Deanship of Research and Graduate Studies at King Khalid University through Large Research Project under RGP2/277/45.

References

1 S. F. Moosavian, Y. Noorollahi and M. Shoaei, *J. Clean. Prod.*, 2024, **439**, 140892.

2 A. Al Ojeery, H. ul Hassan, S. A. Al Balawi, M. W. Iqbal, A. M. Afzal and N. M. A. Hadia, *J. Phys. Chem. Solids*, 2023, **180**, 111473.

3 A. Agrawal, A. Gaur and A. Kumar, *J. Energy Storage*, 2023, **66**, 107395.

4 A. Joseph and T. Thomas, *J. Alloys Compd.*, 2024, **971**, 172714.

5 J. F. Pedrayes, M. F. Quintana, G. A. Orcajo, E. E. V. Zaldivar, M. G. Melero and M. F. Cabanas, *Batteries*, 2024, 10.

6 Suyanto, P. A. Darwito, R. A. Wahyuono, M. S. Arifin and B. Sudarmanta, *Int. J. Automot. Technol.*, 2023, **24**, 187–194.

7 M. A. Dar, S. R. Majid, M. Satgunam, C. Siva, S. Ansari, P. Arularasan and S. Rafi Ahamed, *Int. J. Hydrogen Energy*, 2024, **70**, 10–28.

8 F. Wang, X. Wu, X. Yuan, Z. Liu, Y. Zhang, L. Fu, Y. Zhu, Q. Zhou, Y. Wu and W. Huang, *Chem. Soc. Rev.*, 2017, **46**, 6816–6854.

9 Y. Cao, J. Liang, X. Li, L. Yue, Q. Liu, S. Lu, A. M. Asiri, J. Hu, Y. Luo and X. Sun, *Chem. Commun.*, 2021, **57**, 2343–2355.

10 J. Yan, S. Li, B. Lan, Y. Wu and P. S. Lee, *Adv. Funct. Mater.*, 2020, **30**, 1902564.

View Article Online
DOI: 10.1039/D4MA01199F

11 G. Sriram, G. Hegde, K. Dhanabalan, Y. Kalegowda, D. Mouraliraman, R. S. Vishwanath, M. Kurkuri and T. H. Oh, *J. Energy Storage*, 2024, **94**, 112454.

12 A. Rajapriya, S. Keerthana and N. Ponpandian, eds. C. M. Hussain and M. B. B. T.-S. S. Ahamed, Elsevier, 2023, pp. 65–82.

13 Q. Zhang and B. Wei, *Small*, 2024, **n/a**, 2311957.

14 C. Costentin, T. R. Porter and J. M. Savéant, *ACS Appl. Mater. Interfaces*, 2017, **9**, 8649–8658.

15 F. Escobar-Teran, H. Perrot and O. Sel, *Physchem*, 2023, 3, 355–384.

16 A. Joseph and T. Thomas, ed. R. K. Gupta, Springer Nature Switzerland, Cham, 2024, pp. 1–17.

17 H. Hosseini and S. Shahrokhian, *Chem. Eng. J.*, 2018, **341**, 10–26.

18 C.-C. Hu, W.-C. Chen and K.-H. Chang, *J. Electrochem. Soc.*, 2004, **151**, A281.

19 M. Song, J. Zhao, H. Li, X. Yu, X. Yang, L. Zhang, Z. Yin and X. Wang, *J. Electroanal. Chem.*, 2020, **857**, 113755.

20 X. Xu, W. Wang, W. Zhou and Z. Shao, *Small Methods*, 2018, **2**, 1–35.

21 K. Brezesinski, J. Wang, J. Haetge, C. Reitz, S. O. Steinmueller, S. H. Tolbert, B. M. Smarsly, B. Dunn and T. Brezesinski, *J. Am. Chem. Soc.*, 2010, **132**, 6982–6990.

22 G. F. Liu, P. P. Ma, Y. Qiao, R. H. Xu, D. M. Huang, R. Y. Hu, L. Y. Liu, G. H. Jiang and M. Demir, *J. Energy Storage*, 2022, **52**, 104942.

23 W. W. Zhang, Y. Wang, Y. C. Li and X. Y. Zhang, *J. Ind. Eng. Chem.*, , DOI:https://doi.org/10.1016/j.jiec.2024.04.048.

24 C. Yang, Y. Gan, M. Lee, C. Ren, K. S. Brinkman, R. D. Green and X. Xue, *J. Mater. Chem. A*, 2020, **8**, 10450–10461.

25 X. Lv, H. Chen, W. Zhou, S.-D. Li and Z. Shao, *J. Mater. Chem. A*, 2020, **8**, 11292–11301.

26 H. Zhou, G. Qi, W. Li, W. Song and Z. Yuan, *Langmuir*, ,

View Article Online
DOI: 10.1039/D4MA01199F

DOI:10.1021/acs.langmuir.4c01339.

27 S. Hu, S. Gu, C. Yang, J. Cheng, J. Xu, J. Pu and B. Chi, *J. Power Sources*, 2024, **602**, 234389.

28 S. Li, Y. Liu, C. Cai, K. Xue, L. Bian and S. An, *J. Power Sources*, 2024, **592**, 233932.

29 F. Xiao, X. Zhang, F. Hu and J. Zhang, *Mater. Chem. Phys.*, 2005, **94**, 221–225.

30 M. A. Salguero Salas, J. M. De Paoli, O. E. Linarez Pérez, N. Bajales and V. C. Fuertes, *Microporous Mesoporous Mater.*, 2020, **293**, 109797.

31 H. Li, J. Yu, Y. Gong, N. Lin, Q. Yang, X. Zhang and Y. Wang, *Sep. Purif. Technol.*, 2023, **307**, 122716.

32 D. Gupta, A. Boora, A. Thakur and T. K. Gupta, *Environ. Res.*, 2023, **231**, 116316.

33 K. Y. Park, Y. Seo, K. B. Kim, S. J. Song, B. Park and J. Y. Park, *Enhanced proton conductivity of yttrium-doped barium zirconate with sinterability in protonic ceramic fuel cells*, Elsevier B.V., 2015, vol. 639.

34 M. Irshad, M. Khalid, M. Rafique, N. Ahmad, K. Siraj, R. Raza, M. Sadiq, M. Ahsan, A. Ghaffar and A. Ashfaq, *RSC Adv.*, 2021, **11**, 14475–14483.

35 D. Yun, J. Kim, S.-J. Kim, J.-H. Lee, J.-N. Kim, H. Yoon, J. Yu, M. Kwak, H. Yoon, Y. Cho and C.-Y. Yoo, *Energies*, 2018, **11**, 3083.

36 K.-Y. Park, Y. Seo, K. B. Kim, S.-J. Song, B. Park and J.-Y. Park, *J. Alloys Compd.*, 2015, **639**, 435–444.

37 N. Singh, M. Seshadri, M. S. Pathak and V. Singh, *Solid State Sci.*, 2019, **87**, 163–170.

38 M. D. Gonçalves, P. S. Maram, A. Navrotsky and R. Muccillo, *Ceram. Int.*, 2016, **42**, 13689–13696.

39 A. Majedi, A. Abbasi and F. Davar, *J. Sol-Gel Sci. Technol.*, 2016, **77**, 542–552.

40 J. Luo, J. Zhang, A. Wang, Y. Liu, J. Cheng, Y. Zhao, D. Yan, L. Jia and J. Li, *Int. J. Hydrogen Energy*, 2024, **56**, 871–879.

View Article Online
DOI: 10.1039/D4MA01199F

41 A. S. Salwa, A. E.-S. Ahmed, H. S. Wasly and M. S. Abd El-Sadek, *ECS J. Solid State Sci. Technol.*, 2022, **11**, 103005.

42 A. Modwi, K. K. Taha, L. Khezami, A. S. Al-Ayed, O. K. Al-Duaij, M. Khairy and M. Bououdina, *J. Inorg. Organomet. Polym. Mater.*, 2020, **30**, 2633–2644.

43 W. Zhu, W. Deng, Z. Li, Z.-Y. Shen, X. Shi, F. Song, W. Luo, Z. Wang and Y. Li, *J. Mater. Sci. Mater. Electron.*, 2022, **33**, 26861–26869.

44 D. A. Agarkov, M. A. Borik, G. M. Korableva, A. V Kulebyakin, B. E. Komarov, I. E. Kuritsyna, E. E. Lomonova, F. O. Milovich, V. A. Myzina, V. A. Pankratov, N. Y. Tabachkova and D. M. Zakharov, *J. Solid State Electrochem.*, 2024, **28**, 1901–1908.

45 G. Kimmel, A. Sahartov, Y. Sadia, Z. Porat, J. Zabicky and E. Dvir, *J. Mater. Res. Technol.*, 2021, **12**, 87–99.

46 K. C. Suresh, S. Surendhiran, P. Manoj Kumar, E. Ranjth Kumar, Y. A. S. Khadar and A. Balamurugan, *SN Appl. Sci.*, 2020, **2**, 1735.

47 R. Varghese, C. O. Sreekala, S. Kurian and J. K. Thomas, *J. Mater. Sci. Mater. Electron.*, 2023, **34**, 1–16.

48 M. Mahiuddin and B. Ochiai, *RSC Adv.*, 2021, **11**, 26683–26686.

49 R. Javed, M. Usman, S. Tabassum and M. Zia, *Appl. Surf. Sci.*, 2016, **386**, 319–326.

50 C. V. Restrepo and C. C. Villa, *Environ. Nanotechnology, Monit. Manag.*, 2021, **15**, 100428.

51 M. Baladi, M. Amiri, P. Mohammadi, K. Salih Mahdi, Z. Golshani, R. Razavi and M. Salavati-Niasari, *Arab. J. Chem.*, 2023, **16**, 104646.

52 P. K. Upadhyay, V. K. Jain, S. Sharma, A. K. Shrivastav and R. Sharma, *IOP Conf. Ser. Mater. Sci. Eng.*, , DOI:10.1088/1757-899X/798/1/012025.

53 M. Irshad, N. Kousar, M. B. Hanif, A. N. Tabish, A. Ghaffar, M. Rafique, K. Siraj, Z. Aslam, M. A. Assiri, M. Imran, M. Mosiałek, Z. Zmrhalova and M. Motola, *Sustain. Energy Fuels*, 2022, **6**, 5384–5391.

View Article Online
DOI: 10.1039/D4MA01199F

54 L. Zhang, Y. Yin, Y. Xu, S. Yu and L. Bi, *Sci. China Mater.*, 2022, **65**, 1485–1494.

55 D. Kubba, I. Ahmed, A. Roy, P. Kour, C. S. Yadav, S. K. Sharma, K. Yadav and K. K. Haldar, *ACS Appl. Nano Mater.*, 2024, **7**, 1536–1547.

56 K. Zulfa, B. Zahara, A. Akmal Afkauni, P. Yuniar Diah Maulida, S. Hartati, I. Mulyani, A. Yudhowijoyo, L. Jaya Diguna, M. Haris Mahyuddin, D. Onggo, M. Danang Birowosuto and Arramel, *Mater. Today Proc.*, , DOI:https://doi.org/10.1016/j.matpr.2024.03.058.

57 M. He, M. Alomar, A. S. Alqarni, N. Arshad, M. Akbar, M. Yousaf, M. S. Irshad, Y. Lu and Q. Liu, *Nanomaterials*, , DOI:10.3390/nano13081420.

58 X. Luan, X. Wang, T. Zhang, L. Gan, J. Liu, Y. Zhai, W. Liu, L. Wang and Z. Wang, *Compounds*, 2024, 4, 268–287.

59 R. W. Utami, R. A. Rafsanjani and D. Triyono, *J. Phys. Conf. Ser.*, 2019, **1153**, 0–5.

60 A. J. McQuillan, M. Osawa, D. Peak, B. Ren and Z. Q. Tian, *Pure Appl. Chem.*, 2019, **91**, 2043–2061.

61 S. M. Bashir and H. Idriss, *J. Chem. Phys.*, , DOI:10.1063/1.5140544.

62 M. A. Ahmed, M. S. Selim and M. M. Arman, *Mater. Chem. Phys.*, 2011, **129**, 705–712.

63 M. Sheoran, R. Sharma, S. Chaudhary, A. Dawar, S. Ojha, A. Verma, A. Srivastava and O. P. Sinha, *Appl. Phys. A*, 2023, **129**, 549.

64 L. E. Garcia and M. A. Sozen, *J. Mater. Chem. A*, 2015, 1–12.

65 Y. Belazougui, A. Dib, T. Hadjersi, R. Maizia, A. Thomas and S. Martemianov, *ChemistrySelect*, 2024, **9**, e202400750.

66 J. P. Cheng, S. Q. Gao, P. P. Zhang, B. Q. Wang, X. C. Wang and F. Liu, *J. Alloys Compd.*, , DOI:10.1016/j.jallcom.2020.153984.

67 S. Guo, W. Chen, M. Li, J. Wang, F. Liu and J. P. Cheng, *Electrochim. Acta*, 2018, **271**, 498–506.

68 T. Zhu, S. J. Zheng, Y. G. Chen, J. Luo, H. B. Guo and Y. E. Chen, *J. Mater. Sci.*, 2014, **49**, 6118–6126.

View Article Online
DOI: 10.1039/D4MA01199F

69 C. Li, H. Chen, R. Nie, Y. Yang and H. Zhou, *J. Mater. Sci. Mater. Electron.*, 2023, **34**, 1–14.

70 E. Bilgin Simsek and Ö. Tuna, *J. Phys. Chem. Solids*, 2023, **176**, 111276.

71 E. Smith, S. Škapin and R. Ubic, *J. Alloys Compd.*, 2020, **836**, 155475.

72 N. Lei, Y. Qiao, G. Liu, R. Xu, G. Jiang, M. Demir and P. Ma, *Mater. Chem. Phys.*, 2022, **288**, 126389.

73 Y. Qiao, G. Liu, R. Xu, R. Hu, L. Liu, G. Jiang, M. Demir and P. Ma, *Electrochim. Acta*, 2023, **437**, 141527.

74 J. He, Y. Zhou, S. Wu, L. Jin, J. Cao, M. Demir and P. Ma, *Inorg. Chem.*, 2024, **63**, 13755–13765.

75 Y. Wu, X. Jia, H. Zhang, F. Zhou, Z. Fu, X. Jia, Z. Li, F. Liu, L. Wang and Z. Xiao, *J. Energy Storage*, 2023, **62**, 106855.

76 O. Karaman, İ. A. Kariper, S. Korkmaz, H. Karimi-Maleh, M. Usta and C. Karaman, *Fuel*, 2022, **328**, 125298.

77 M. Abdullah, P. John, K. F. Fawy, S. Manzoor, K. Y. Butt, A. G. Abid, M. Messali, M. Najam-Ul-Haq and M. N. Ashiq, *RSC Adv.*, 2023, **13**, 12009–12022.

78 T. N. V. Raj, P. A. Hoskeri, H. B. Muralidhara, C. R. Manjunatha, K. Y. Kumar and M. S. Raghu, *J. Electroanal. Chem.*, 2020, **858**, 113830.

79 Z. U. Rehman, M. A. Raza, A. Tariq, U. N. Chishti, M. F. Maqsood, N. Lee, M. H. Awais, S. M. Z. Mehdi and A. Inam, *J. Energy Storage*, 2020, **32**, 101951.

80 P. M. Shafi, N. Joseph, A. Thirumurugan and A. C. Bose, *Chem. Eng. J.*, 2018, **338**, 147–156.

81 S. Nayak, A. A. Kittur and S. Nayak, *Curr. Res. Green Sustain. Chem.*, 2022, **5**, 100292.

82 M. Riaz, S. M. Ali, S. D. Ali, M. Sadiq and M. A. Shakoori, *Diam. Relat. Mater.*, 2024, **144**, 110938.

83 R. Kumar, S. Gokul, F. Ran, S. Sambasivam, K. A. Alrashidi and R. Thangappan, *J. Energy*

View Article Online
DOI: 10.1039/D4MA01199F

Storage, 2024, **98**, 113231.

View Article Online
DOI: 10.1039/D4MA01199F

Data Availability Statement

The data will be made available upon request

Dr. Muneeb Irshad